Atomic Layer Deposition of Crystalline MoS2 Thin Films : New Molybdenum Precursor for Low-Temperature Film Growth

Mattinen, Miika

2017-09-22

Mattinen , M , Hatanpaa , T , Sarnet , T , Mizohata , K , Meinander , K , King , P J , Khriachtchev , L , Räisänen , J , Ritala , M & Leskelä , M 2017 , ' Atomic Layer Deposition of Crystalline MoS2 Thin Films : New Molybdenum Precursor for Low-Temperature Film Growth ' , Advanced Materials Interfaces , vol. 4 , no. 18 , 1700123 . https://doi.org/10.1002/admi.201700123

http://hdl.handle.net/10138/301614
https://doi.org/10.1002/admi.201700123

acceptedVersion

DOI: 10.1002/admi.201700123
Article type: Full Paper

Atomic Layer Deposition of Crystalline MoS_2 Thin Films: New Molybdenum Precursor for Low-Temperature Film Growth

Miika Mattinen, Timo Hatanpää, Tiina Sarnet,[§] Kenichiro Mizohata, Kristoffer Meinander, Peter J. King, Leonid Khriachtchev, Jyrki Räisänen, Mikko Ritala, Markku Leskelä*

M. Mattinen, T. Hatanpää, Dr. T. Sarnet, Dr. P. King, Dr. L. Khriachtchev, Prof. M. Ritala, Prof. M. Leskelä
Department of Chemistry, University of Helsinki, P.O. Box 55, FI-00014, Finland
E-mail: mikko.ritala@helsinki.fi
Dr. K. Mizohata, Dr. K. Meinander, Prof. J. Räisänen
Department of Physics, University of Helsinki, P.O. Box 43, FI-00014, Finland
§ Present address: Picosun Oy, Masalantie 365, FI-02430, Masala, Finland

Keywords: 2D materials, atomic layer deposition, MoS_2, thin films

Molybdenum disulfide (MoS_2) is a semiconducting 2D material, which has evoked wide interest due to its unique properties. However, the lack of controlled and scalable methods for production of MoS_2 films at low temperatures remains a major hindrance on its way to applications. In this work, atomic layer deposition (ALD) is used to deposit crystalline MoS_2 thin films at a relatively low temperature of 300 °C. A new molybdenum precursor, $Mo(thd)_3$ (thd=2,2,6,6-tetramethylheptane-3,5-dionato), is synthesized, characterized, and used for film deposition with H_2S as the sulfur precursor. Self-limiting growth with a low growth rate of approximately 0.025 Å cycle^{-1}, straightforward thickness control, and large-area uniformity are demonstrated. Film crystallinity is found to be relatively good considering the low deposition temperature, but the films have significant surface roughness. Additionally, chemical composition as well as optical and wetting properties are evaluated. MoS_2 films are deposited on a variety of substrates, which reveal notable differences in growth rate, surface

morphology, and crystallinity. The growth of crystalline MoS_2 films at comparably low temperatures by ALD contributes towards the use of MoS_2 for applications with a limited thermal budget.

1. Introduction

In the last 10 years, transition metal dichalcogenides (TMDCs) have received considerable attention as a promising material group for a variety of applications. The intriguing layered, two-dimensional (2D) crystal structures of TMDCs give birth to unique properties in thin (<10 nm) TMDC layers that are not seen in their bulk form. This is due to quantum confinement effects and the weakness of interlayer interactions in TMDCs.[1–4] To date, molybdenum disulfide (MoS_2) has been the most extensively studied TMDC material.

Compared to the most well-known 2D material, graphene, which is a semi-metal, the semiconducting 2H phase of MoS_2 is advantageous in having a band gap suitable for electronic applications. In bulk form, MoS_2 has an indirect band gap of 1.3 eV, which increases as a function of decreasing film thickness. In monolayer MoS_2 (thickness ~0.6 nm), the band gap becomes direct with a width of 1.8 eV.[1] Importantly, to meet the requirements of different applications, properties of MoS_2 and other TMDCs can be tuned by controlling the thickness,[1] doping and alloying,[5–8] surface modification and functionalization,[9–11] strain,[12,13] and by creating heterostructures with other 2D materials.[6,14–16]

The appealing properties of TMDCs have led to a wide range of proposed applications. MoS_2 has been extensively studied as a channel material in conventional field-effect transistors[17–21] as well as phototransistors and other optoelectronic devices.[16,21,22] The 2D structure of TMDCs plays a crucial role in possible applications relying on more exotic quantum phenomena, such as valleytronics.[23,24] MoS_2 has also shown promise in, for example, catalysis,[25] batteries,[26] photovoltaics,[27] sensors,[28] and medicine.[29]

The production of high-quality, large-area MoS_2 films with a thickness controllable down to a monolayer, as required in many of the aforementioned applications, still remains a major

challenge. Additionally, in many cases, the processing temperature should be kept as low as possible in order to avoid damaging sensitive substrates, such as polymers or nanostructures. Initially, flakes of monolayer MoS_2 were produced from natural MoS_2 crystals using micromechanical exfoliation, a top-down method capable of producing high-quality monolayers, albeit with poor throughput as well as limited control over flake thickness and dimensions.[4,30,31] Liquid-phase exfoliation of bulk crystals, on the other hand, offers good scalability, but often suffers from limited flake size, poor crystallinity, or contamination.[4,31,32]

Bottom-up methods offer a more controllable way to produce MoS_2 films. High-quality MoS_2 thin films are most commonly deposited by chemical vapor deposition (CVD) or sulfurization of metal or metal oxide thin films. The most common CVD procedure utilizes MoO_3 and sulfur as precursors.[33–36] Unfortunately, the low vapor pressure of MoO_3 sets limitations to both the deposition temperature (typically 650 to 850 °C) and deposition area (typically no more than 1 cm^2).[34,36] Sulfurization of Mo or MoO_x films also requires high temperatures, usually 500 to 1000 °C.[36–39] Although upscaling of the sulfurization method appears to be easier compared to the MoO_3-based CVD, sulfurization tends to produce films of lower quality.[34,36,37] Other bottom-up techniques used for the deposition of thin MoS_2 films include sputtering,[40] physical vapor transport (PVT),[41] pulsed laser deposition (PLD),[42] and atomic layer deposition (ALD).[43–52]

Atomic layer deposition is an inherently scalable technique that can be regarded as an advanced modification of CVD. It is based on self-limiting surface reactions of vapor-phase precursors that are alternately pulsed to substrates. In order to avoid uncontrolled gas-phase reactions, the precursor pulses are separated by purge or evacuation steps. The self-limiting reactions often allow deposition of high-quality films at comparatively low deposition temperatures, typically 100 to 400 °C. ALD offers large-area uniformity, precise control over

film thickness as well as unmatched conformality, i.e. uniform thickness over substrates with complex three-dimensional shapes.[53–55] So far, ALD of MoS_2 has been reported using $MoCl_5$ with H_2S,[43–46] as well as $Mo(CO)_6$ with H_2S,[47,52] H_2S plasma,[48] or dimethyl disulfide.[49–51] The films deposited with $Mo(CO)_6$ have mostly been amorphous due to the low deposition temperatures of 100 to 200 °C,[47,49–51] although the films deposited with H_2S plasma were polycrystalline.[48] Using $MoCl_5$ and H_2S, crystalline MoS_2 films have been deposited by ALD,[43–46] but a post-deposition annealing[43,46] or high deposition temperatures in excess of 500 °C[45] have still been required, in most cases, to obtain films of sufficient quality. Thus, there is a clear need to develop new ALD processes for MoS_2.

In this study, we report the preparation of crystalline MoS_2 films by ALD at a relatively low temperature of 300 °C, using a new molybdenum precursor, tris(2,2,6,6-tetramethylheptane-3,5-dionato)molybdenum(III), $Mo(thd)_3$, with H_2S as the sulfur precursor. We describe the synthesis of $Mo(thd)_3$ and other Mo(III) β-diketonates and evaluate their thermal properties. Growth of MoS_2 films shows typical characteristics of ALD: self-limited growth with linear thickness control and excellent film uniformity. Detailed characterization provides information on film growth, morphology, crystallinity, and composition as well as optical properties and wettability. Film growth is demonstrated and studied on a range of different substrates.

2. Results and discussion

2.1. Precursor selection, synthesis, and evaluation

2.1.1. Evaluation of published MoS_2 processes

We started the study by evaluating the known $MoCl_5$+H_2S process[43–46] in our commercial hot-wall, flow-type ALD reactor.[56] Despite testing a range of deposition conditions, for example temperatures from 150 to 500 °C, we either obtained no films at all or the films were highly non-uniform in thickness across the substrates. Increasing the $MoCl_5$ dose decreased the film thickness close to the precursor inlet, which hints towards etching of the deposited film by $MoCl_5$. Later, we also found that $Mo(CO)_6$, the other molybdenum precursor used for ALD of MoS_2,[47–52] suffered from heavy precursor decomposition in our reactor already at 110 °C. This was avoided by lowering the temperature below 100 °C, but no film deposition was found in this case.

We attribute these results to the design of the ALD reactor used in this work,[56] where the precursors undergo multiple collisions with hot walls and substrates, increasing the possibility of film etching and precursor decomposition. Additionally, the precursor source design based on inert gas valving[56] may increase the likelihood of thermal decomposition compared to many other ALD reactors, where the precursors are usually heated in separate containers.

2.1.2 Synthesis and evaluation of Mo(III) β-diketonates

Due to the failures with the published processes, we searched for alternative Mo precursors. Interestingly, although metal β-diketonates are commonly used in ALD and CVD, there are, to the best of our knowledge, no reports on using Mo precursors containing only β-diketonate ligands. In general, reports of Mo(III) coordination compounds, especially β-diketonates, are rare. Compared to the more commonly investigated Mo(VI) precursors, the oxidation state +III may be beneficial, as it is closer to the oxidation state +IV in MoS_2.

$Mo(thd)_3$ was synthesized using a reaction between $MoCl_3(THF)_3$[57] and three equivalents of Kthd or Lithd. Surprisingly, this simple metathesis reaction has not been previously reported for making Mo β-diketonates. After isolation and purification by sublimation, $Mo(thd)_3$ was obtained as dark brown, air sensitive solid with yields up to 83%. Crystal structure of the compound solved by single crystal X-ray diffraction (XRD) shows individual $Mo(thd)_3$ molecules (**Figure 1a)**. Detailed information on the crystal structure and its comparison to the previously reported Mo(III) β-diketonates are provided in Supporting Information.

Thermogravimetric analysis (TG) was used to evaluate thermal properties of $Mo(thd)_3$ as well as similarly synthesized $Mo(acac)_3$ and $Mo(hfac)_3$ (Figure 1b). The low residual masses of 0.3 and 2.6%, respectively, for $Mo(thd)_3$ and $Mo(hfac)_3$ imply evaporation of the compounds. In agreement with previous studies, $Mo(acac)_3$ seemed to mainly decompose, which may be explained by the intermolecular O···H interactions found in its crystal structure.[58]

Three steps were found in the TG curve of $Mo(thd)_3$: first, there was a small mass loss between 80–150 °C due to evaporation of some free Hthd. Major, 95% weight loss step associated with evaporation of $Mo(thd)_3$, was seen at 150–265 °C. At 265–300 °C a small, 3% weight loss step was seen, likely due to evaporation of an oxidized species $MoO_2(thd)_2$. The first and third steps were attributed to decomposition and oxidation of $Mo(thd)_3$, respectively, during loading of the TG sample in air.

The TG curve measured for $Mo(hfac)_3$ was similar to that measured for $Mo(thd)_3$, but the weight losses occurred at approximately 100 °C lower temperatures. This indicates that $Mo(hfac)_3$ is well volatile, but in our studies the thermal stability of the compound seemed to be lower than that of $Mo(thd)_3$. Also, for thin film growth, fluorinated ligands raise the question of possible F contamination in the resulting films. Thus, $Mo(thd)_3$ was chosen for the film growth studies.

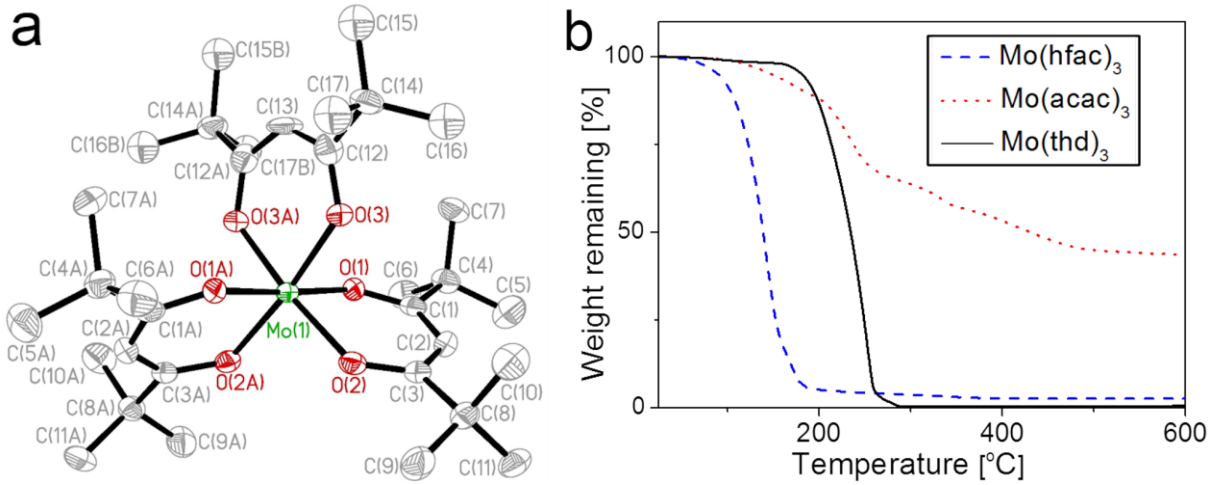

Figure 1. Mo β-diketonates. a) Molecular structure of $Mo(thd)_3$ solved by single crystal XRD. Thermal ellipsoids are drawn on the 30% probability level. Hydrogen atoms are omitted for clarity. b) TG curves for synthesized Mo β-diketonates.

2.2. Film growth on silicon

Based on initial growth trials, 300 °C was chosen as the most promising deposition temperature for ALD of MoS_2 using $Mo(thd)_3$ and H_2S. In growth experiments on native oxide terminated silicon, saturation of the growth rate was achieved with $Mo(thd)_3$ and H_2S pulses of at least 0.5 and 2.0 s, respectively (**Figure 2a,b**). The growth rates were calculated from film thicknesses measured by energy-dispersive X-ray spectrometry (EDX), assuming smooth and uniform films with bulk density (5.06 g cm^{-3})[59]. The saturation indicates that the precursors react with the surface in self-limiting manner, which is characteristic for ALD. Varying the purge time after each precursor pulse between 0.5 and 2.0 s caused no change in the growth rate, which further confirms the ALD-like behavior of the process. Purge times of 1.0 s and pulse times of 0.5 s for $Mo(thd)_3$ and 2.0 s for H_2S were used in the following depositions, unless otherwise noted.

Film thickness increased linearly with increasing number of deposition cycles, although some nucleation delay appeared to be present, as the line fitted to the thickness values did not pass through the origin (Figure 2c). Growth rate of 0.028 Å $cycle^{-1}$ and nucleation delay of 150 cycles were determined from the slope and the intersection of the fitted line with the abscissa, respectively.

The lowest temperature where film growth was observed was 250 °C, where the growth rate was only approximately 0.005 Å $cycle^{-1}$ (Figure 2d). When increasing the deposition temperature, the growth rate increased up to 300 °C, where the majority of depositions were performed, and then decreased again when going to 325 °C. At 350 °C slight $Mo(thd)_3$ decomposition was visible in the glass source tubes of the ALD reactor, and the extent of decomposition was clearly larger at 400 °C.

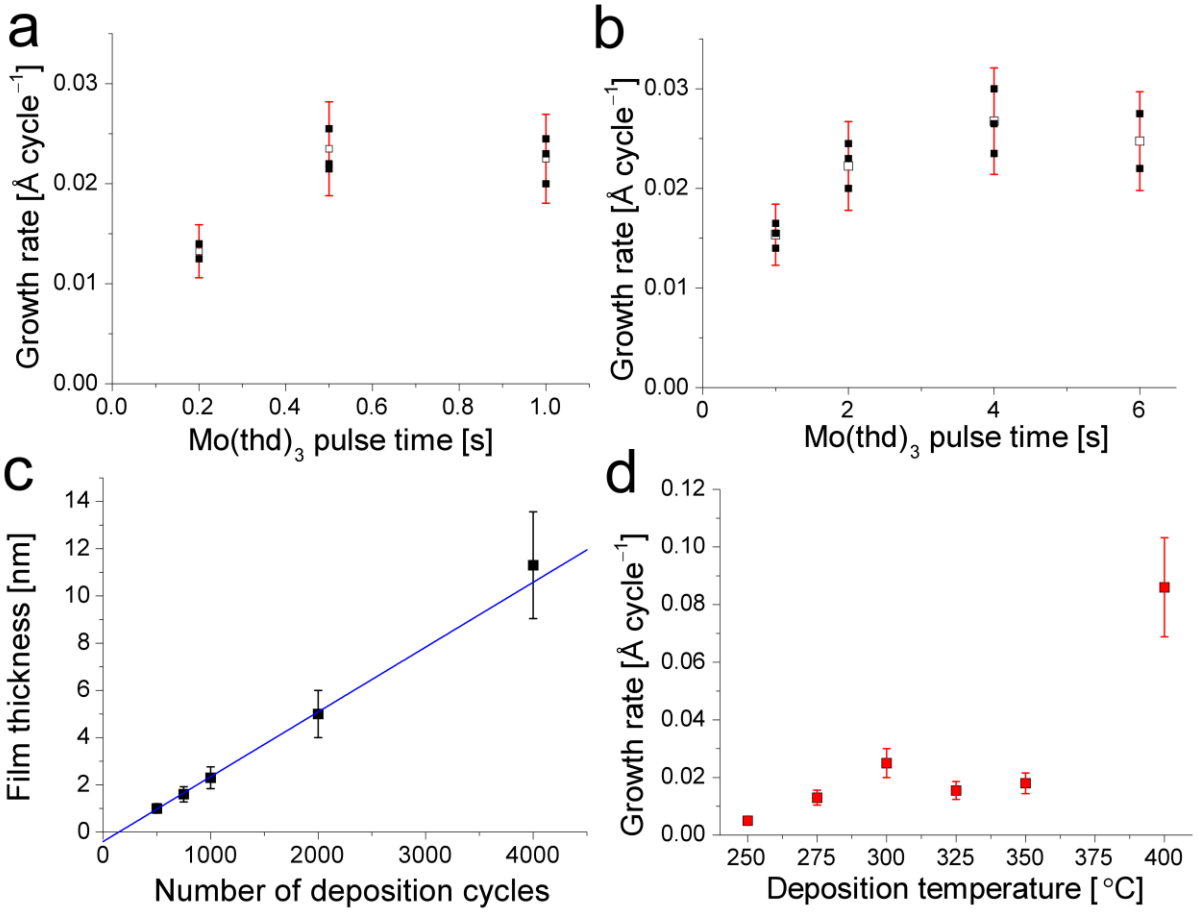

Figure 2. MoS_2 film growth. Growth rate versus a) $Mo(thd)_3$ and b) H_2S pulse length. c) Film thickness versus number of ALD cycles. d) Growth rate versus deposition temperature. The filled and open symbols refer to single measurements and average values, respectively. Unless otherwise noted, 2000 cycles were applied at 300 °C on silicon substrates, using 0.5 s (c,d) or 1 s (b) $Mo(thd)_3$ pulses, 2 s H_2S pulses and 1 s purges.

The observed growth rate was low, approximately 0.025 Å cycle^{-1}. In general, two main reasons have been proposed to limit the growth rate in ALD: steric hindrance between the adsorbed precursor molecules, and limited number of reactive sites on the surface.[53] Relatively low growth rates have often been observed when using bulky metal thd precursors. For example, saturated growth rates of about 0.20 Å cycle^{-1} and 0.15 Å cycle^{-1} were reported using $Ni(thd)_2$[60] and $La(thd)_3$[61], respectively, with H_2S.

The much smaller growth rate found in this work suggests that the density of reactive sites is more likely the limiting factor. For many ALD oxide processes, hydroxyl (-OH) groups are the major reactive sites,[62] whereas the analogous thiol (-SH) groups can play an important role for sulfides. As an example, Meng et al.[63] found a rapid decrease in the density of thiol

groups, and, consequently, in the ALD growth rate of GaS_x deposited from $Ga_2(NMe_2)_6$ and H_2S, when increasing the deposition temperature from 125 to 225 °C.

The density of thiol groups, at least on the most common, sulfur-terminated, (002) basal planes of MoS_2 can be expected to be small based on the studies on MoS_2 catalysts.[64] The edges of basal plane-terminated, typically platelike crystallites, on the other hand, contain dangling bonds and may act as reactive sites, as may also other kinds of defect sites. Thus, it is possible that the film growth proceeds mainly on the edges and defects, which could explain the slow growth.

2.3. Characterization of films deposited on silicon

2.3.1. Morphology

The evolution of film morphology with increasing film thickness was analyzed with scanning electron microscopy (SEM, **Figure 3a**) and atomic force microscopy (AFM, Figure 3b). The surface remained smooth and featureless up to 250 cycles, which may be due to the nucleation delay noted above. After 500 cycles, small crystallites or particles appeared, and the film seemed to be discontinuous at this point. This is expected, as nucleation delay is often connected to island growth in ALD.[65] The flake-like morphology with the crystallites standing up from the substrate became more pronounced with increasing number of deposition cycles. The apparent lateral grain size estimated from the SEM and AFM images increased slightly with increasing number of deposition cycles, from approximately 10 to 30 nm.

The evolution of film roughness (Figure 3c) can yield useful information on the film growth. The small grain size and considerable roughness make it difficult to determine from the SEM and AFM images when a continuous or closed film is formed, and although the morphology is also a challenge for AFM roughness measurements, the small decrease in roughness between 750 and 1000 cycles may indicate the formation of a continuous film, as demonstrated by the simulations of ALD film growth by Nilsen et al.[66,67] as well as experimental observations on HfO_2[68] and Pt[69] ALD films, for example.

Additional information on the surface morphology can be obtained by examination of line profiles taken from the AFM images (Figure 3d). In a film grown with 500 cycles, for example, there are height differences of up to 3 nm, which is to be compared with the average film thickness of approximately 1 nm. This shows the extent of film roughness caused by the flakes standing up from the substrate plane, which is detrimental for applications requiring smooth films, for example electronics. However, some applications, such as electrochemical

hydrogen evolution,[25,70] and batteries[26] may also benefit from large film roughness and films exposing the crystallite edges and interlayer spaces.

In thin film growth the film morphology is first controlled by nucleation and later by grain growth processes. Nucleation of ALD films can be sensitive to the deposition chemistry and conditions, including factors such as precursors and their pulse times, substrate and its preparation, and deposition temperature. The orientation of the formed nuclei can then affect or even determine the film morphology. Furthermore, if the film growth mainly occurs on edges and defect sites of MoS_2 crystallites, as suggested in Section 2.2, this could lead to the perceived fairly random orientation of crystallites. Thus, even if the initially formed nuclei have their basal (002) planes oriented parallel to the substrate, their orientation can change with increasing film thickness.

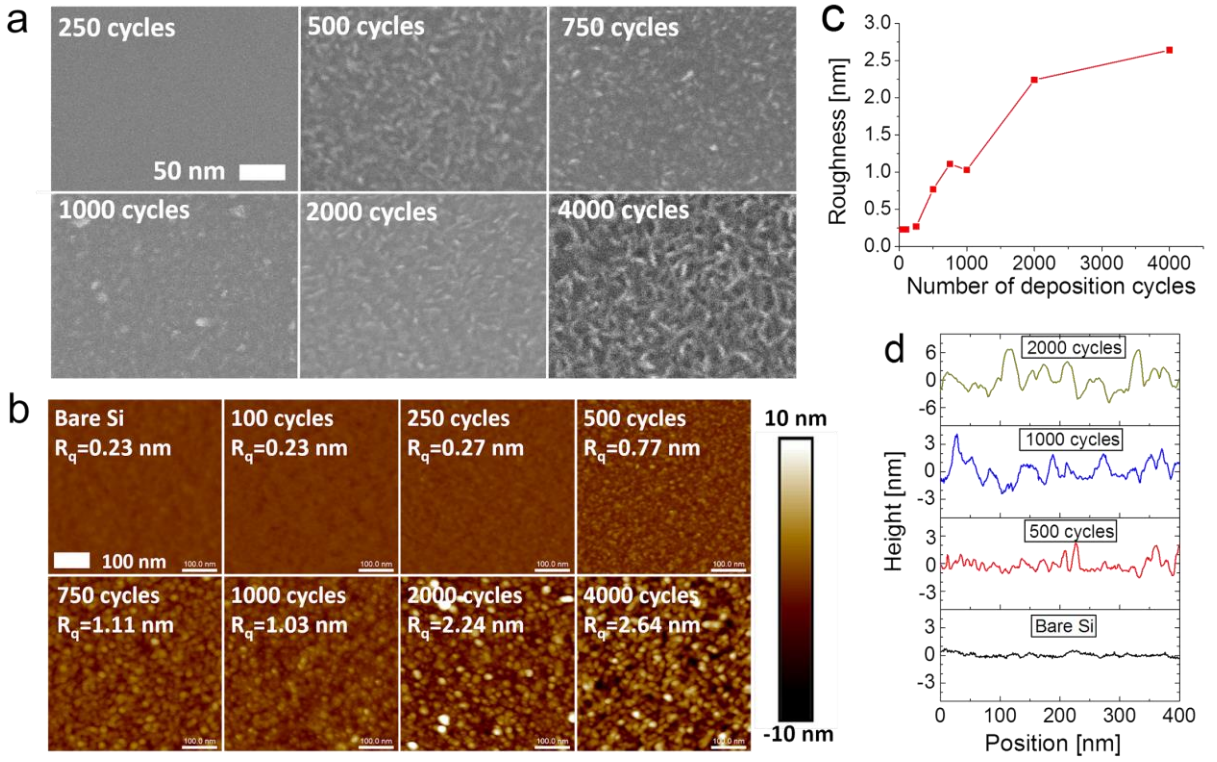

Figure 3. Surface morphology of MoS_2 films. a) SEM images of MoS_2 films grown with 250 to 4000 cycles. b) AFM images and film roughness (R_q) of Si substrate and MoS_2 films grown with 100 to 4000 cycles. c) Film roughness versus number of deposition cycles. d) Representative AFM line profiles of Si substrate and MoS_2 films grown with 500, 1000, and 2000 cycles. All of the films were deposited at 300 °C on Si.

2.3.2. Crystallinity

We studied the crystallinity of the films using XRD and Raman spectroscopy. In grazing incidence XRD, a peak corresponding to the (002) plane of the desired, semiconducting 2H phase of MoS_2,[71] was detected after 1000 cycles (**Figure 4a**). After 4000 cycles, weak peaks corresponding to the (100) or (101) as well as the (110) planes were also detected. The improvement of the crystallinity with increasing number of deposition cycles is evident in the decreasing width of the (002) peak.

Raman spectroscopy is a powerful method for studying TMDCs, as it can provide information on crystal structure (phase), electronic structure, strain, and film thickness, among others.[72] The films studied with Raman measurements were deposited on 90 nm SiO_2/Si substrates, where the SiO_2 layer is close to the quarter-wave thickness of the 488 nm laser, and gives a strong signal enhancement for thin films on top,[73] including MoS_2.[74] We note that the film growth was very similar on both 90 nm SiO_2 and native oxide covered silicon, as will be discussed in Section 2.4. After only 500 deposition cycles, we observed intense peaks at 384 and 406 cm^{-1}, which correspond to the E^1_{2g} and A_{1g} vibrations of 2H-MoS_2, respectively (Figure 4b).[72,75] The intensity of these two peaks did not increase monotonously with increasing film thickness, in accordance with some previous studies.[75,76] However, the intensity of the Si peak at 520 cm^{-1}, which originates from the substrate below the MoS_2 and SiO_2 layers, expectedly decreased with increasing MoS_2 film thickness.

Interestingly, we observed no change in the peak positions or separation (22 cm^{-1}) when the film thickness increased from approximately 1 nm (500 cycles) to 5 nm (2000 cycles). This is in contrast to the typically observed blue shift of E^1_{2g} and red-shift of A_{1g} peak with decreasing film thickness in few-layer MoS_2.[75] The lack of peak shifts may result from coexistence of MoS_2 crystallites with different thicknesses, due to the initial island-like film growth.

As we observed asymmetric broadening of the MoS_2 peaks, we used the peak fitting strategy of Mignuzzi et al.[77] to estimate disorder in the films. In addition to the E^1_{2g} and A_{1g} modes, three disorder-induced peaks were fitted, which originate from the transverse optical (TO, ~355 cm^{-1}), longitudinal optical (LO, ~377 cm^{-1}), and out-of-plane optical (ZO, ~412 cm^{-1}) branches at the **M** point of the Brillouin zone (Figure 4c). The relatively large integrated intensity of these modes compared to the E^1_{2g} and A_{1g} modes indicates the presence of disorder in the deposited films, which is expected for a relatively low deposition temperature.

The full width at half-maximum (FWHM) values of the fitted E^1_{2g} and A_{1g} components were approximately 6 and 7 cm^{-1}, respectively, whereas those for the full peaks (i.e. without deconvolution) were around 9 cm^{-1} for all of the measured films. Mechanically exfoliated, as well as the best CVD-grown monolayer MoS_2-films deposited at 650 °C or above have shown FWHMs as low as 3–4 cm^{-1}.[33,78] On the other hand, for the ALD MoS_2 films deposited from $MoCl_5$ and H_2S at 475 °C, the E^1_{2g} FWHM was as broad as 18 cm^{-1}, which decreased by sulfur annealing to 12 cm^{-1} (720 °C) or even 4.2 cm^{-1} (920 °C).[46] A four-monolayer MoS_2 film, produced by sulfurization of a MoO_x film, yielded E^1_{2g} FWHM of 6.5 cm^{-1} at 750 °C, whereas a higher sulfurization temperature of 1000 °C reduced the FWHM to 4.6 cm^{-1}.[39] In summary, the Raman spectra indicate comparably good crystallinity, especially considering the low deposition temperature of 300 °C.

Finally, multiple measurements were performed from different positions of the ~5 cm^2 SiO_2 substrate (Figure 4d). Identical peak intensities at all positions, including the Si substrate peak, confirm that the films have excellent thickness uniformity, as is expected for ALD.

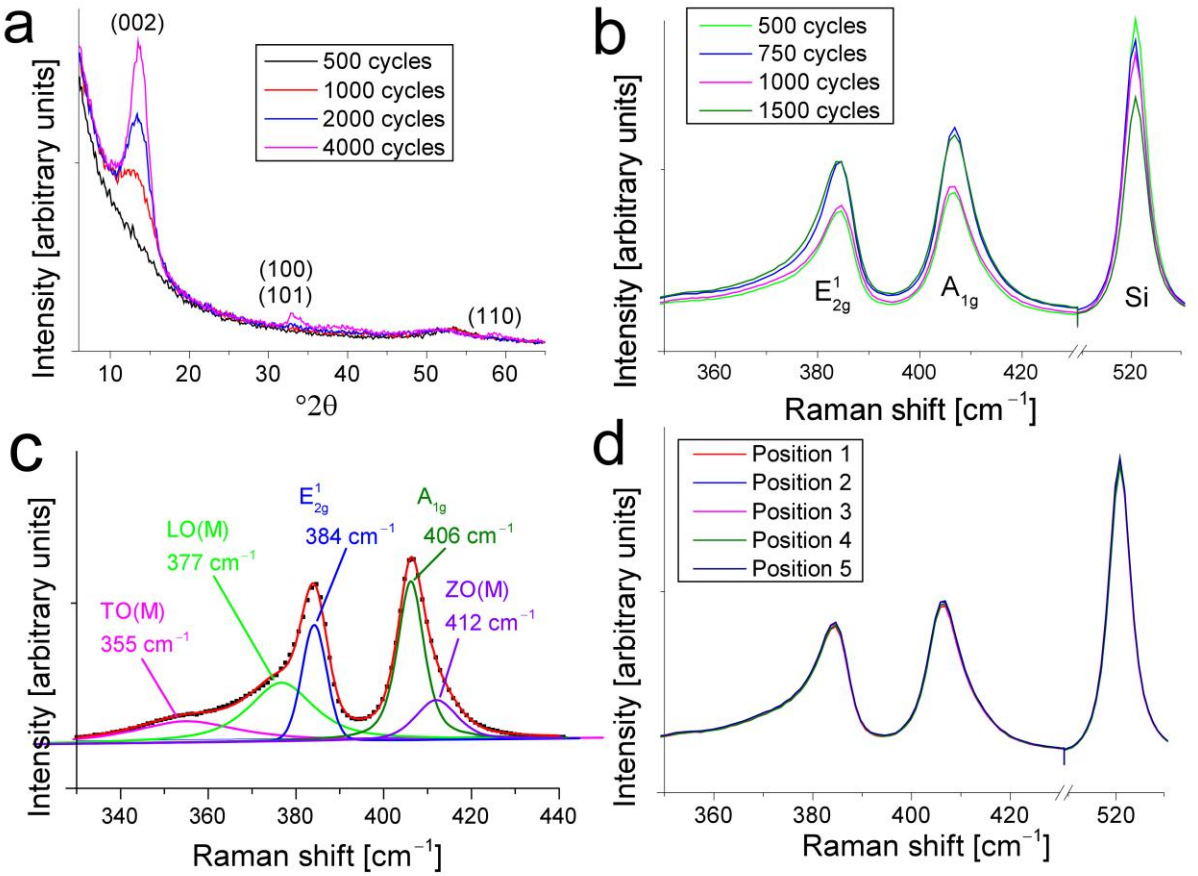

Figure 4. Crystallinity of MoS_2 films. a) X-ray diffractograms of films grown with 500 to 4000 cycles. b) Raman spectra of films grown with 500 to 1500 cycles. c) Peak fitting of different Raman modes in Raman spectrum of a 1000 cycle film. d) Raman spectra from different positions of a 1000 cycle film on a 2.3×2.3 cm^2 substrate. All of the films were deposited at 300 °C. Si and 90 nm SiO_2/Si substrates were used for XRD and Raman measurements, respectively.

We also explored how the deposition temperature affects film crystallinity. As noted earlier, self-limiting growth seemed to occur between 250 and 325 °C. The crystallinity of the deposited films seemed to improve with increasing deposition temperature, based on SEM images (**Figure 5a**) and X-ray diffractograms (Figure 5b). Although a clear increase in grain size was evident at 350 °C, and especially at 400 °C, these films were not deposited under pure ALD conditions. The film deposited at 400 °C consisted of thin flakes standing up from the substrate with a length of approximately 100 nm, for a nominal film thickness of about 20 nm. Deposition of highly crystalline MoS_2 films by ALD appears to call for more thermally stable molybdenum precursors.

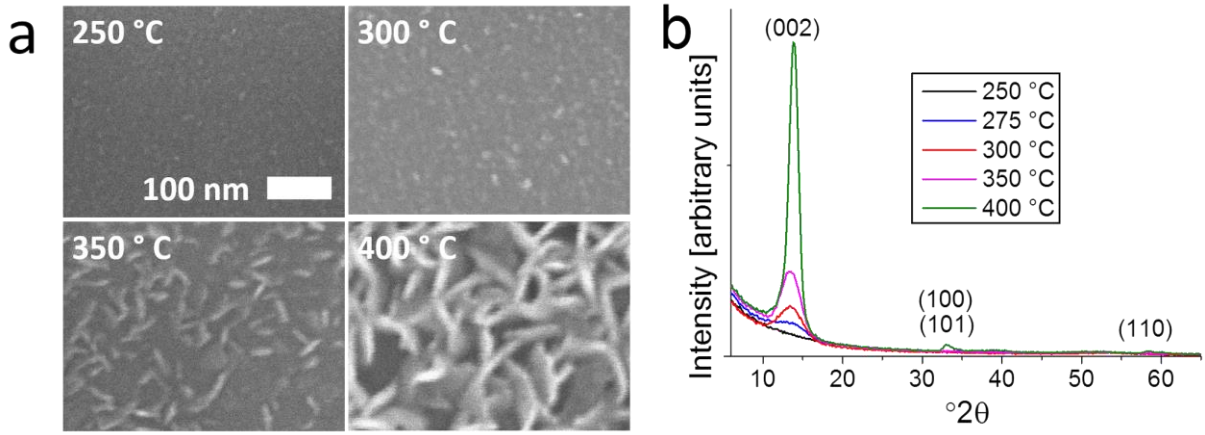

Figure 5. Effect of deposition temperature on film crystallinity. a) SEM images and b) X-ray diffractograms of MoS_2 films grown at different temperatures on silicon using 2000 cycles.

2.3.3. Composition

X-ray photoelectron spectroscopy (XPS) was used to study the composition and chemical bonding on the film surface, i.e. no sputtering was done. A survey scan (Figure S2a and Table S3 in Supporting Information) revealed peaks originating from Mo, S, O, C, and Sn. Additionally, time-of-flight elastic recoil detection analysis (ToF-ERDA) provided information on film composition averaged throughout the film thickness, detecting also hydrogen and a small amount of nitrogen in addition to the abovementioned elements (Table S3 in Supporting Information). It should be noted, however, that due to the small thickness of the analyzed film (~10 nm) as well as the rough morphology, the film surface, the film-substrate interface, and the native SiO_2 layer likely make a notable contribution to the ToF-ERDA results.

High-resolution X-ray photoelectron spectra from the Mo 3d region (**Figure 6a**) showed a doublet corresponding to Mo $3d_{5/2}$ at 229.9 eV and Mo $3d_{3/2}$ at 233.1 eV. The observed binding energies are amongst those reported for thin 2H-MoS_2 layers and films (231.6 to 233.2 eV for Mo $3d_{3/2}$)[39,43,44,47–49,51,52,40]. In addition, about 10% of the molybdenum was present as oxidized MoO_3 (Mo^{6+}) with binding energies[79] of 233.4 and 236.6 eV for Mo $3d_{5/2}$ and Mo $3d_{3/2}$, respectively. This implies that the film surface is at least partially oxidized in

air. The sulfur/molybdenum atomic ratio of 1.7 (ToF-ERDA) is in agreement with fairly stoichiometric MoS_2 with some surface oxidation. S 2s peak was also observed near the Mo 3d doublet at 227.1 eV, in good agreement with the binding energy of S^{2-} in 2H-MoS_2.[39,43,44,47]

Binding energies of S $2p_{3/2}$ (162.7 eV) and S $2p_{1/2}$ (163.9 eV) seen in Figure 6b are also within the range of values reported for 2H-MoS_2.[39,43,44,47–49,51,52,40] Additionally, weak doublets at 161.8 and 163.3 eV as well as 163.9 and 165.1 eV were assigned to Sn-S[80] and C-S bonding, respectively. Carbon and oxygen were present in multiple chemical environments, as revealed by their broad peaks (Figure S2b,c in Supporting Information). It appears likely that most of the carbon, as well as the hydrogen observed by ToF-ERDA, originate from surface hydrocarbon contamination, although the presence of some residual thd ligands or their fragments cannot be excluded. The oxygen is likely due to surface oxidation, atmospheric contamination, and native SiO_2 layer, the last one affecting ToF-ERDA results only.

A small amount of tin present in the films (approximately 1–3% of the amount of molybdenum) was assigned to be present as tin(IV)sulfide species (Figure 6b and Figure S2d in Supporting Information). Tin is a residue from the synthesis of the $Mo(thd)_3$ precursor, where metallic tin was used as a reducing agent.

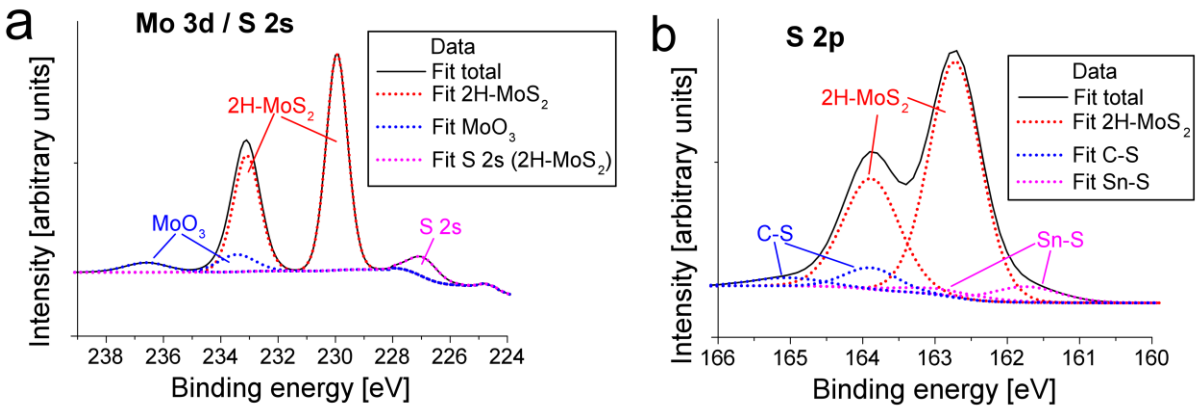

Figure 6. X-ray photoelectron spectra. a) Mo 3d / S 2s region. b) S 2p region. The analyzed film was deposited on silicon at 300 °C using 4000 cycles.

2.3.4. Other film properties

We also studied the wettability of the deposited films, and observed the water contact angle to increase with increasing film thickness from slightly hydrophilic (80° after 100 cycles) to hydrophobic (above 100° after 4000 cycles) as a consequence of increased roughness. More detailed results can be found in Supporting Information. Optical properties of the films deposited on glass substrates will be discussed in Section 2.4.3.

2.4. Films on other substrates

2.4.1. Film growth

We evaluated a range of different substrates to see how the film growth, surface morphology, and crystallinity are affected by the substrate. As ALD is based on surface reactions, the substrate often has an effect on the film growth in the nucleation stage, which can further alter the resulting film properties. Compared to the already discussed native oxide covered silicon, the other tested substrates can be roughly divided into three groups in terms of the growth rate (**Table 1**): enhanced growth with more than doubled growth rate was seen on soda lime glass, whereas smaller enhancement was found on ALD-SnS and, surprisingly, HF-treated silicon (Si-H) substrates. On the other hand, ALD-Al_2O_3 and ALD-Ir substrates showed inhibited growth. On majority of the tested substrates (90 or 300 nm SiO_2, borosilicate glass, sapphire, indium tin oxide (ITO) coated glass, ALD-ZnS, and ALD-SnO_2), the growth rate was similar to Si.

We speculate that the enhanced growth on soda lime glass could be due to interfacial mixing, i.e. diffusion of some of the substrate cations, especially Na, into the film. This could affect precursor adsorption and, furthermore, growth rate. We note that borosilicate glass, which was found to contain Al, B, Ba, Ca, Si, Sr, Zn, and W cations, but no alkali metals, yielded growth rate similar to silicon. We also found that film growth saturated on soda lime glass, although with longer $Mo(thd)_3$ pulses compared to Si, with the saturated growth rate being approximately four times that on silicon (Figure S5a,b in Supporting Information). The growth was also linear with respect to the number of deposition cycles on both silicon and soda lime glass, thus excluding nucleation effects as an explanation for the different growth rates (Figure S5c in Supporting Information).

Inhibited growth on ALD-Al_2O_3 may be explained by surface "poisoning" by β-diketonate ligands, which has been found to hinder nucleation of ALD NiS[60] and SnS[81] on ALD-Al_2O_3. In other words, Al-thd or Al-Mo-thd surface groups formed after the adsorption of $Mo(thd)_3$

appear to be unreactive towards H_2S. Interestingly, film growth on sapphire (α-Al_2O_3) was more facile than on amorphous ALD-Al_2O_3, which could be due to different bonding of the thd-ligand to these surfaces. The inhibited growth on ALD-Ir may stem from the high catalytic activity of iridium, as decomposition of $Mo(thd)_3$ into a carbonaceous layer on iridium could inhibit further adsorption of the precursor, and terminate the film growth.

Table 1. MoS_2 film growth rate, surface roughness, and XRD (002) FWHM on different substrates. 2000 cycles were applied at 300 °C.

Substrate	Growth rate [Å cycle^{-1}]	Roughness [nm]	XRD (002) FWHM [°]
Si (native oxide)	0.025±0.005	2.2	3.2
Enhanced growth			
Soda lime glass	0.065 (0.11[a)])	2.4	2.7
ALD-SnS	0.041	-[b)]	2.9
Si-H	0.036	4.2	3.3
Growth rate similar to Si			
SiO_2	0.025	2.1	2.9
Borosilicate glass	0.025	3.7	3.0
Sapphire	0.023	2.4	4.5
ITO coated glass	0.030	-[b)]	-[c)]
ALD-ZnS	0.023	-[b)]	-[c)]
ALD-SnO_2	0.026	-[b)]	-[c)]
Inhibited growth			
ALD-Al_2O_3	<0.005[d)]	1.8	-[c)]
ALD-Ir	<0.005[d)]	-[b)]	-[c)]

[a)]With 1 s $Mo(thd)_3$ pulse, instead of 0.5 s; [b)] Not measured; [c)] No peak; [d)] Film thickness below the detection limit of approximately 1 nm

2.4.2. Film morphology and crystallinity

In addition to the growth rate, film morphology, roughness, and crystallinity were also affected by the substrate choice. Morphology was evaluated from SEM (Figure S6 in Supporting Information) and, for selected substrates, AFM images (Figure S7 in Supporting

Information). AFM images were also used for calculating film roughness. Crystallinity was estimated from the FWHM of the (002) XRD reflection of MoS_2 (Figure S8 in Supporting Information). As is well known, peak width increases with decreasing crystallite size, although it can also be affected by other factors, such as strain.

Films on Si and SiO_2 were found to be similar in terms of morphology, roughness, and crystallinity, which is expected considering that our silicon substrates were covered by a native silicon oxide layer. Regarding the substrates with enhanced growth, films on soda lime glass had crystallinity and roughness similar to Si, when comparing films with similar thicknesses. Thus, it appears that if any mixing with soda lime glass substrate occurs, it does not deteriorate film crystallinity. The film grown on hydrogen-terminated silicon (Si-H) was the roughest out of all of the substrates studied by AFM, which may at least partially explain the somewhat higher growth rate compared to Si. In terms of crystallinity, films on Si-H and ALD-SnS also appeared to be similar to Si.

Of the substrates with growth rates similar to Si, films on borosilicate glass and sapphire showed similar and weaker crystallinity, respectively, compared to Si. The film on borosilicate glass was quite rough due to larger flakes scarcely present on the surface. For the films on ALD-SnO_2, ALD-ZnS, and ITO coated glass no signs of crystallinity were detected by XRD. On the substrates with inhibited growth (ALD-Al_2O_3 and ALD-Ir), no signs of crystallinity were detected, although there were small features visible on ALD-Al_2O_3 in AFM and SEM images. For some of the substrates, especially ITO coated glass and ALD-SnO_2, and, to a smaller degree, ALD-SnS, ALD-ZnS, and ALD-Ir, the inherent roughness and morphology of the substrates hindered reliable examination of the MoS_2 morphology.

2.4.3. Optical properties on glass substrates

We studied the optical properties of MoS_2 films deposited on soda lime and borosilicate glass substrates. As the film morphology and crystallinity on these substrates were similar to films

on silicon, we assume that the optical properties should also be similar. The transmittances of the bare glass substrates were quite similar to each other, as were the general shapes of the transmittance curves of the MoS_2-covered substrates (**Figure 7a**). The two broad features marked with asterisks at 610 and 660 nm were assigned to characteristic A and B exciton peaks of 2H-MoS_2, respectively.[82]

Using a Tauc plot we obtained an indirect band gap of 1.2 eV for a 2000 cycle film on borosilicate glass (Figure 7b), in agreement with the generally accepted value of 1.3 eV for bulk MoS_2. Band gaps of 1.2±0.2 eV were measured for films of different thickness (1000 to 8000 cycles, corresponding to approximately 5 to 50 nm) on soda lime glass. Band gap determination of films thinner than about 5 nm was not successful using this method and equipment. Therefore, we were unable to observe the increase in band gap with decreasing thickness that is commonly found for few-layer MoS_2.[1]

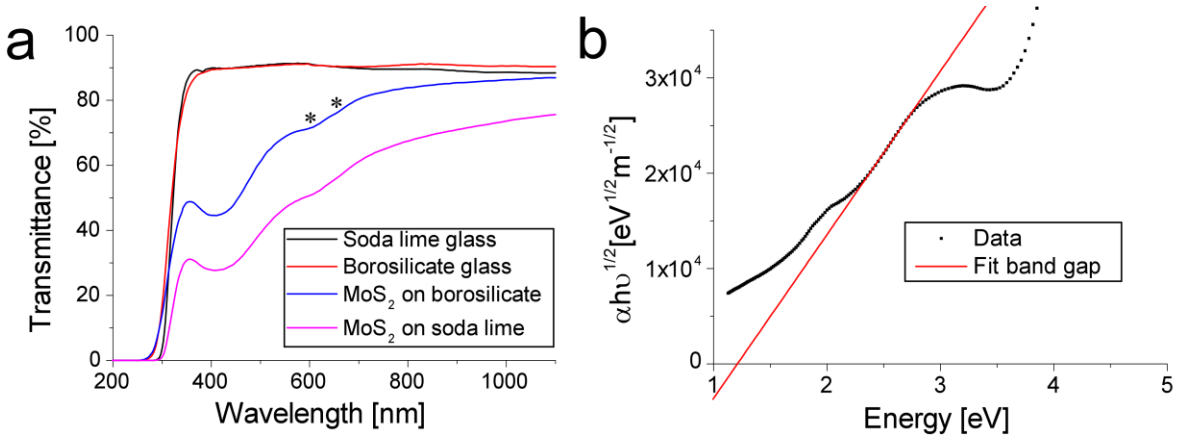

Figure 7. Optical properties of MoS_2 films. a) UV-VIS transmittance spectra for bare and MoS_2-covered soda lime and borosilicate glass substrates. b) Tauc plot for a MoS_2 film on borosilicate glass. The films were deposited at 300 °C using 2000 cycles.

3. Conclusion

In this work, we deposited crystalline MoS_2 thin films by ALD using a new molybdenum precursor, $Mo(thd)_3$, together with H_2S at 300 °C. Self-limiting growth and linear film thickness control, characteristic of ALD, were demonstrated. We characterized the films using a variety of techniques. The films were found to be rather rough, consisting of flake-like grains with size of approximately 10 to 30 nm. Raman spectroscopy revealed the film crystallinity to be relatively good, especially taking the low deposition temperature into account. Compositional studies showed some surface oxidation and contamination, but the films themselves were estimated to be close to stoichiometric MoS_2. Optical and wetting properties of the films were also analyzed, showing properties expected for MoS_2. We deposited MoS_2 films on different substrates, and although the growth was successful on most of them, there were marked differences in the film growth, morphology, and crystallinity. The current work offers an alternative for deposition of crystalline MoS_2 films at modest deposition temperatures compared to alternative deposition methods.

4. Experimental Section

Precursor synthesis and characterization: All handling and manipulations were done under rigorous exclusion of air and moisture using standard Schlenk techniques and inert gas (N_2 or Ar) glove box. Hexane and toluene were dried over 4 Å molecular sieves while Et_2O and THF were freshly distilled from sodium benzophenone ketyl. $MoCl_5$ (99.6%, anhydrous, Strem), KH 30 wt-% dispersion in mineral oil (Aldrich), and Hthd (98%, Strem) were used as received. Kthd was prepared by reacting KH with Hthd in THF. $MoCl_3(THF)_3$ was prepared by reducing $MoCl_5$ with Sn pellets using a method modified from the one introduced by Stoffelbach et al.[57]

Thermogravimetric analysis was performed using a Mettler Toledo Star^e system equipped with a TGA850 thermobalance. The measurements were done at atmospheric pressure using N_2 (50 ml min^{-1}) as the purge gas. Heating rate was 10 °C min^{-1} and the sample size was 10±1 mg. Melting points were taken from the single differential thermal analysis (SDTA) data measured by the thermobalance. Mass spectra were recorded with a JEOL JMS-SX102 instrument operating in electron impact mode (70 eV) using a direct insertion probe and a sublimation temperature range of 50–300 °C.

$Mo(thd)_3$: In a 600 ml Schlenk bottle $MoCl_3(THF)_3$ (12.95 g, 30.90 mmol) was suspended in THF (200 ml). This solution was cooled to −10 °C with an ice/acetone bath and THF solution (200 ml) of Kthd (20.59 g, 92.69 mmol) was added using a Teflon cannula and argon pressure. The solution was allowed to warm to room temperature and left to stir over night. THF was evaporated using a warm water bath and vacuum. The resulting dark brown solid was transferred into a sublimator and sublimed at 160 °C / 0.5 mbar. The sublimate being the product, $Mo(thd)_3$, it was collected in a glove box. The yield of the highly air sensitive, dark brown solid was 16.60 g (83%). m.p. 149 °C.

MS: *m/*z 647 (M^+) with the correct isotopic pattern. In addition, several fragment ions were seen. Ions with oxygen, like $[Mo(thd)_2O_2]^+$, $[Mo(thd)_2O]^+$, $[Mo(thd)_2O_2 - {}^tBu]^+$ and

$[Mo(thd)O_2]^+$ were also seen, but these were most likely due to exposure to air during loading the sample into the mass spectrometer.

NMR was not resolvable because the compound was paramagnetic. Details of the crystal structure determination can be found in the Supporting Information. CCDC 1526595 contains the supplementary crystallographic data for this paper. These data can be obtained free of charge from The Cambridge Crystallographic Data Centre via www.ccdc.cam.ac.uk/data_request/cif.

Film deposition: A commercial, flow-type F-120 ALD reactor[56] (ASM Microchemistry) was used for the deposition of MoS_2 thin films under a pressure of about 5 mbar. Nitrogen (N_2, AGA, 99.999%) at a flow rate of 400 sccm was used as carrier gas as well as for purging. $Mo(thd)_3$ was sublimed from an open glass boat held at 115 °C, and pulsed with inert gas valving. Hydrogen sulfide (H_2S, Messer-Griesheim, 99.99%) was fed into the reactor through needle and solenoid valves with its flow rate adjusted to 7 sccm during continuous flow. Purges of 1 s were used between the precursor pulses, whereas $Mo(thd)_3$ and H_2S pulse lengths of 0.5 and 2 s were used, unless otherwise noted. Temperatures from 250 to 400 °C were explored, with the optimal temperature of 300 °C used in most depositions.

Films were mostly deposited on 5 × 5 cm^2 silicon and soda lime glass substrates. The native oxide of silicon was not removed, unless otherwise noted. Piranha treatment and solvent cleaning of the silicon substrates was tested, but no major difference in film growth was found; thus, the normal procedure only included removal of particles by a blow of pressurized nitrogen. Some depositions were performed on HF-treated, hydrogen-terminated silicon (Si-H), SiO_2 with a thickness of 90 or 300 nm, borosilicate glass, indium tin oxide (ITO) coated glass, c-plane sapphire as well as different ALD films (Al_2O_3, SnO_2, SnS, and ZnS). Of the

ALD films, Al_2O_3, SnS, and ZnS were deposited immediately before the MoS_2 deposition in the same ALD reactor, i.e. without a vacuum break.

Film characterization: Film thicknesses were measured by EDX (Oxford INCA 350 connected to a Hitachi S-4800 SEM). The EDX spectra were measured at 20 keV and an optimization procedure was used to determine the beam current as well as the spectrometer gain under the same measurement conditions. GMRFilm program[83] was used to calculate the film thickness and composition from the measured k-ratios of the Mo Lα and S Kα X-ray lines using the phi-rho-Z (PAP) matrix correction. Smooth and uniform films and a MoS_2 bulk density[59] of 5.06 g cm^{-3} were assumed in the calculations. Due to the difficulty in separating the Mo and S X-ray lines, the EDX measurement uncertainty was estimated to be 20%.

Film morphology was studied by SEM (Hitachi S-4800) and AFM (Veeco Multimode V). Silicon probes with nominal tip radius of less than 10 nm (Bruker) were used for the tapping-mode AFM imaging in air. AFM images were flattened or planefitted to minimize the effects of sample tilt and scanner nonlinearity. Roughness was calculated as a root-mean-square value (R_q). Bruker Nanoscope 1.5 software was used for image modification and analysis.

Composition of the surface layers was analyzed by XPS using an Argus Spectrometer (Omicron NanoTechnology GmbH) operating at a pass energy of 20 eV. Samples were illuminated with X-rays emitted from a standard Mg source (Kα line) at a photon energy of 1253.6 eV. Binding energies were calibrated using the C 1s peak (284.8 eV) of ambient hydrocarbons, and peak fitting was done using the CasaXPS software. Film composition averaged throughout the film thickness was analyzed by ToF-ERDA using a 40 MeV $^{127}I^{7+}$ ion beam.[84]

Film crystallinity was probed with XRD (PANalytical X'Pert Pro MPD) using grazing incidence geometry (incident angle of 1°) and Cu Kα radiation (λ = 1.54 Å). To determine the FWHM, XRD peaks were fit with Gaussian functions. Micro-Raman spectra were recorded in

a back-scattering scheme with a confocal Raman microscope (Horiba Jobin Yvon LabRam HR 800) using excitation at 488 nm of an argon-ion laser (2.5 mW on the sample), a 100× objective, and spectral resolution of 2 cm^{-1}. The total acquisition time was 100 s. Peak fitting was conducted using Pseudo-Voigt function implemented in OriginPro 8.6.

Optical transmission measurements using a UV-VIS spectrophotometer (Hitachi U-2000) were used to construct Tauc plots and determine the band gaps of films deposited on borosilicate and soda lime glass substrates. Resistance measurements were performed using a four-point probe (CPS probe station connected to a Keithley 2400 SourceMeter). Static water contact angles were measured with a Cam 100 instrument from KSV Instruments using de-ionised water.

Supporting Information
Supporting Information is available from the Wiley Online Library or from the author.

Acknowledgements
The research was supported by ASM Microchemistry and the Finnish Centre of Excellence in Atomic Layer Deposition funded by Academy of Finland. Mr. Mikko Heikkilä and Dr. Marianna Kemell are thanked for assistance with the XRD and EDX measurements, respectively. Dr. Elena Cianci and Dr. Silvia Vangelista from Laboratorio MDM, IMM-CNR, Italy, are acknowledged for help in trials with the $Mo(CO)_6$ precursor.

Received: ((will be filled in by the editorial staff))
Revised: ((will be filled in by the editorial staff))
Published online: ((will be filled in by the editorial staff))

References

[1] K. F. Mak, C. Lee, J. Hone, J. Shan, T. F. Heinz, *Phys. Rev. Lett.* **2010**, *105*, 136805.

[2] W. Zhao, R. M. Ribeiro, G. Eda, *Acc. Chem. Res.* **2015**, *48*, 91.

[3] M. Chhowalla, H. S. Shin, G. Eda, L.-J. Li, K. P. Loh, H. Zhang, *Nat. Chem.* **2013**, *5*, 263.

[4] Y. P. V. Subbaiah, K. J. Saji, A. Tiwari, *Adv. Funct. Mater.* **2016**, *26*, 2046.

[5] A. A. Tedstone, D. J. Lewis, P. O'Brien, *Chem. Mater.* **2016**, *28*, 1965.

[6] H. Wang, H. Yuan, S. S. Hong, Y. Li, Y. Cui, *Chem. Soc. Rev.* **2014**, *44*, 2664.

[7] J.-G. Song, G. H. Ryu, S. J. Lee, S. Sim, C. W. Lee, T. Choi, H. Jung, Y. Kim, Z. Lee, J.-M. Myoung, C. Dussarrat, C. Lansalot-Matras, J. Park, H. Choi, H. Kim, *Nat. Commun.* **2015**, *6*, 7817.

[8] Y. Chen, J. Xi, D. O. Dumcenco, Z. Liu, K. Suenaga, D. Wang, Z. Shuai, Y.-S. Huang, L. Xie, *ACS Nano* **2013**, *7*, 4610.

[9] S. Presolski, M. Pumera, *Mater. Today* **2015**, *19*, 140.

[10] M. Amani, R. A. Burke, X. Ji, P. Zhao, D.-H. Lien, P. Taheri, G. H. Ahn, D. Kiriya, J. W. Ager III, E. Yablonovitch, J. Kong, M. Dubey, A. Javey, *ACS Nano* **2016**, *10*, 6535.

[11] X. Chen, A. R. McDonald, *Adv. Mater.* **2016**, 28, 5738.

[12] A. Castellanos-Gomez, R. Roldán, E. Cappelluti, M. Buscema, F. Guinea, H. S. J. van der Zant, G. A. Steele, *Nano Lett.* **2013**, *13*, 5361.

[13] H. J. Conley, B. Wang, J. I. Ziegler, R. F. Haglund Jr., S. T. Pantelides, K. I. Bolotin, *Nano Lett.* **2013**, *13*, 3626.

[14] S. Bertolazzi, D. Krasnozhon, A. Kis, *ACS Nano* **2013**, *7*, 3246.

[15] X. Duan, C. Wang, J. C. Shaw, R. Cheng, Y. Chen, H. Li, X. Wu, Y. Tang, Q. Zhang, A. Pan, J. Jiang, R. Yu, Y. Huang, X. Duan, *Nat. Nanotechnol.* **2014**, *9*, 1024.

[16] W. Zhang, Q. Wang, Y. Chen, Z. Wang, A. T. S. Wee, *2D Mater.* **2016**, *3*, 022001.

[17] F. Schwierz, J. Pezoldt, R. Granzner, *Nanoscale* **2015**, *7*, 8261.

[18] B. Radisavljevic, A. Radenovic, J. Brivio, V. Giacometti, A. Kis, *Nat. Nanotechnol.* **2011**, *6*, 147.

[19] J. Li, M. Östling, *Electronics* **2015**, *4*, 1033.

[20] Y. Yoon, K. Ganapathi, S. Salahuddin, *Nano Lett.* **2011**, *11*, 3768.

[21] D. Jariwala, V. K. Sangwan, L. J. Lauhon, T. J. Marks, M. C. Hersam, *ACS Nano* **2014**, *8*, 1102.

[22] K. F. Mak, J. Shan, *Nat. Photonics* **2016**, *10*, 216.

[23] D. Xiao, G.-B. Liu, W. Feng, X. Xu, W. Yao, *Phys. Rev. Lett.* **2012**, *108*, 196802.

[24] H. Zeng, J. Dai, W. Yao, D. Xiao, X. Cui, *Nat. Nanotechnol.* **2012**, *7*, 490.

[25] D. M. Andoshe, J.-M. Jeon, S. Y. Kim, H. W. Jang, *Electron. Mater. Lett.* **2015**, *11*, 323.

[26] X. Wang, Q. Weng, Y. Yang, Y. Bando, D. Golberg, *Chem. Soc. Rev.* **2016**, *45*, 4042.

[27] X. Yu, K. Sivula, *ACS Energy Lett.* **2016**, *1*, 315.

[28] K. Kalantar-zadeh, J. Z. Ou, *ACS Sensors* **2015**, *1*, 5.

[29] Y. Chen, L. Wang, J. Shi, *Nano Today* **2016**, *11*, 292.

[30] K. S. Novoselov, D. Jiang, F. Schedin, T. J. Booth, V. V Khotkevich, S. V Morozov, A. K. Geim, *Proc. Natl. Acad. Sci. U. S. A.* **2005**, *102*, 10451.

[31] F. Bonaccorso, A. Lombardo, T. Hasan, Z. Sun, L. Colombo, A. C. Ferrari, *Mater. Today* **2012**, *15*, 564.

[32] X. Zhang, Z. Lai, C. Tan, H. Zhang, *Angew. Chem.* **2016**, 128, 8960; *Angew. Chem. Int. Ed.* **2016**, *55*, 8816.

[33] Y.-H. Lee, X.-Q. Zhang, W. Zhang, M.-T. Chang, C.-T. Lin, K.-D Chang, Y.-C. Yu, J. T.-W. Wang, C.-S. Chang, L.-J. Li, T.-W. Lin, *Adv. Mater.* **2012**, *24*, 2320.

[34] H. F. Liu, S. L. Wong, D. Z. Chi, *Chem. Vap. Deposition* **2015**, *21*, 241.

[35] M. Bosi, *RSC Adv.* **2015**, *8*, 75500.

[36] S. L. Wong, H. Liu, D. Chi, *Prog. Cryst. Growth Charact. Mater.* **2016**, *62*, 9.

[37] R. Gatensby, T. Hallam, K. Lee, N. McEvoy, G. S. Duesberg, *Solid-State. Electron.* **2016**, *125*, 39.

[38] Y. Zhan, Z. Liu, S. Najmaei, P. M. Ajayan, J. Lou, *Small* **2012**, *8*, 966.

[39] S. Vangelista, E. Cinquanta, C. Martella, M. Alia, M. Longo, A. Lamperti, R. Mantovan, F. B. Basset, F. Pezzoli, A. Molle, *Nanotechnology* **2016**, *27*, 175703.

[40] J.-H. Huang, H.-H. Chen, P.-S. Liu, L.-S. Lu, C.-T. Wu, C.-T. Chou, Y.-J. Lee, L.-J. Li, W.-H. Chang, T.-H. Hou, *Mater. Res. Express* **2016**, *3*, 065007.

[41] S. Wu, C. Huang, G. Aivazian, J. S. Ross, D. H. Cobden, X. Xu, *ACS Nano* **2013**, *7*, 2768.

[42] M. I. Serna, S. H. Yoo, S. Moreno, Y. Xi, J. P. Oviedo, H. Choi, H. N. Alshareef, M. J. Kim, M. Minary-Jolandan, M. A. Quevedo-Lopez, *ACS Nano* **2016**, *10*, 6054.

[43] L. K. Tan, B. Liu, J. H. Teng, S. Guo, H. Y. Low, K. P. Loh, *Nanoscale* **2014**, *6*, 10584.

[44] R. Browning, P. Padigi, R. Solanki, D. J. Tweet, P. Schuele, D. Evans, *Mater. Res. Express* **2015**, *2*, 035006.

[45] Y. Kim, J.-G. Song, Y. J. Park, G. H. Ryu, S. J. Lee, J. S. Kim, P. J. Jeon, C. W. Lee, W. J. Woo, T. Choi, H. Jung, H.-B.-R. Lee, J.-M. Myoung, S. Im, Z. Lee, J.-H. Ahn, J. Park, H. Kim, *Sci. Rep.* **2016**, *6*, 18754.

[46] A. Valdivia, D. J. Tweet, J. F. Conley Jr, *J. Vac. Sci. Technol. A* **2016**, *34*, 021515.

[47] D. K. Nandi, U. K. Sen, D. Choudhury, S. Mitra, S. K. Sarkar, *Electrochim. Acta* **2014**,

146, 706.

[48] Y. Jang, S. Yeo, H.-B.-R. Lee, H. Kim, S.-H. Kim, *Appl. Surf. Sci.* **2016**, *365*, 160.

[49] Z. Jin, S. Shin, D. H. Kwon, S.-J. Han, Y.-S. Min, *Nanoscale* **2014**, *6*, 14453.

[50] S. Shin, Z. Jin, D. H. Kwon, R. Bose, Y.-S. Min, *Langmuir* **2015**, *31*, 1196.

[51] D. H. Kwon, Z. Jin, S. Shin, W.-S. Lee, Y.-S. Min, *Nanoscale* **2016**, *8*, 7180.

[52] J. J. Pyeon, S. H. Kim, D. S. Jeong, S.-H. Baek, C.-Y. Kang, J.-S. Kim, S. K. Kim, *Nanoscale* **2016**, *8*, 10792.

[53] M. Ritala, J. Niinistö, in *Chemical Vapour Deposition: Precursors, Processes and Applications* (Eds.: A.C. Jones, M.L. Hitchman), Royal Society Of Chemistry, Cambridge, U.K., **2009**, Ch. 4, pp. 158–206.

[54] R. W. Johnson, A. Hultqvist, S. F. Bent, *Mater. Today* **2014**, *17*, 236.

[55] S. M. George, *Chem. Rev.* **2010**, *110*, 111.

[56] T. Suntola, *Thin Solid Films* **1992**, *216*, 84.

[57] F. Stoffelbach, D. Saurenz, R. Poli, *Eur. J. Inorg. Chem.* **2001**, 2699.

[58] A. Y. Ledneva, S. B. Artemkina, D. A. Piryazev, V. E. Fedorov, *J. Struct. Chem.* **2015**, *56*, 1021.

[59] *CRC Handbook of Chemistry and Physics*, 97th ed. (Online), CRC Press, Boca Raton, FL, http://hbcpnetbase.com, accessed: December, 2016

[60] N. Mahuli, S. K. Sarkar, *J. Vac. Sci. Technol. A* **2016**, *34*, 01A142.

[61] K. Kukli, H. Heikkinen, E. Nykänen, L. Niinistö, *J. Alloys Compd.* **1998**, *275–277*, 10.

[62] K. Knapas, M. Ritala, *Crit. Rev. Solid State Mater. Sci.* **2013**, *38*, 167.

[63] X. Meng, J. A. Libera, T. T. Fister, H. Zhou, J. K. Hedlund, P. Fenter, J. W. Elam, *Chem. Mater.* **2014**, *26*, 1029.

[64] J. V. Lauritsen, F. Besenbacher, *J. Catal.* **2015**, *328*, 49.

[65] R. L. Puurunen, *J. Appl. Phys.* **2005**, *97*, 121301.

[66] O. Nilsen, O. B. Karlsen, A. Kjekshus, H. Fjellvåg, *Thin Solid Films* **2007**, *515*, 4527.

[67] O. Nilsen, O. B. Karlsen, A. Kjekshus, H. Fjellvåg, *Thin Solid Films* **2007**, *515*, 4538.

[68] K. Kolanek, M. Tallarida, M. Michling, D. Schmeisser, *J. Vac. Sci. Technol. A* **2012**, *30*, 01A143.

[69] X. Jiang, T. M. Gür, F. B. Prinz, S. F. Bent, *Chem. Mater.* **2010**, *22*, 3024.

[70] Q. Ji, Y. Zhang, J. Shi, J. Sun, Y. Zhang, Z. Liu, *Adv. Mater.* **2016**, 6207.

[71] PDF 00-037-1492, JCPDS-ICDD, International Center for Diffraction Data

[72] X. Zhang, Q.-H. Tan, J.-B. Wu, W. Shi, P.-H. Tan, *Nanoscale* **2016**, *8*, 6435.

[73] L. Y. Khriachtchev, R. Lappalainen, M. Räsänen, *Diam. Relat. Mater.* **1998**, *7*, 1451.

[74] H. Zhang, Y. Wan, Y. Ma, W. Wang, Y. Wang, L. Dai, *Appl. Phys. Lett.* **2015**, *107*, 101904.

[75] H. Li, Q. Zhang, C. C. R. Yap, B. K. Tay, T. H. T. Edwin, A. Olivier, D. Baillargeat, *Adv. Funct. Mater.* **2012**, *22*, 1385.

[76] X.-L. Li, X.-F. Qiao, W.-P. Han, X. Zhang, Q.-H. Tan, T. Chen, P.-H. Tan, *Nanotechnology* **2016**, *27*, 145704.

[77] S. Mignuzzi, A. J. Pollard, N. Bonini, B. Brennan, I. S. Gilmore, M. A. Pimenta, D. Richards, D. Roy, *Phys. Rev. B: Condens. Matter Mater. Phys.* **2015**, *91*, 195411.

[78] Y. Yu, C. Li, Y. Liu, L. Su, Y. Zhang, L. Cao, *Sci. Rep.* **2013**, *3*, 1866.

[79] N. M. D. Brown, N. Cui, A. McKinley, *Appl. Surf. Sci.* **1998**, *134*, 11.

[80] T. J. Whittles, L. A. Burton, J. M. Skelton, A. Walsh, T. D. Veal, V. R. Dhanak, *Chem. Mater.* **2016**, *28*, 3718.

[81] J. Y. Kim, S. M. George, *J. Phys. Chem. C* **2010**, *114*, 17597.

[82] A. R. Beal, J. C. Knights, W. Y. Liang, *J. Phys. C: Solid State Phys.* **1972**, *5*, 3540.

[83] R. A. Waldo, in *Microbeam Analysis* (Ed.: D.E. Newbury), San Francisco Press, San Francisco, **1988**, pp. 310–314.

[84] J. Jokinen, J. Keinonen, P. Tikkanen, A. Kuronen, T. Ahlgren, K. Nordlund, *Nucl. Instruments Methods Phys. Res. Sect. B* **1996**, *119*, 533.